Combustion and Flame 262 (2024) 113339

Contents lists available at ScienceDirect

Combustion and Flame

journal homepage: www.sciencedirect.com/journal/combustion-and-flame

Multichannel kinetics of methoxymethyl + O_2 in combustion

Qian Zhao, Wuchuan Sun, Yingjia Zhang *, Zuohua Huang *

State Key Laboratory of Multiphase Flow in Power Engineering, Xi'an Jiaotong University, Xi'an 710049, China

ARTICLE INFO

Keywords:
Ab initio calculations
Dimethyl ether
Low-temperature oxidation
Kinetics
RRKM/Master equation

ABSTRACT

Organic peroxy radicals ($R\dot{O}_2$), formed by association reaction of $\dot{R}$ + O_2, are important intermediates in low-temperature combustion of hydrocarbon fuels. A fate of $R\dot{O}_2$ is isomerize to QOOH, and the downstream reactions of QOOH are known to profoundly fuel reactivity. However, both experimental measurements and high-level theoretical calculations of $R\dot{O}_2$ kinetics are scarce, leading to a large gap in our understanding of $R\dot{O}_2$ fate. In this study, methoxy-methyl-peroxy radical ($CH_3OCH_2O\dot{O}$) is investigated as a model compound to elucidate the fate of $R\dot{O}_2$. Based on a high-level quantum chemical calculation and RRKM/master equation calculation, we report a detailed $R\dot{O}_2$ unimolecular reaction surface, as well as the corresponding temperature- and pressure-dependent rate coefficients. All the calculated results can be used to estimate the corresponding rate coefficients of larger oxygen-centered fuels and to construct the chemical kinetic model of dimethyl ether in combustion science.

1. Introduction

Oxidation of biogenic and anthropogenic organic compounds in such disparate processes as ozone/secondary organic aerosol (SOA) formation in Earth's troposphere and fuel autoignition in combustion systems is governed by a surprisingly similar set of reactive intermediates [1–3]. An important and ubiquitous class of intermediate is the organic peroxy radical $R\dot{O}_2$. In the atmospheric, the autoxidation of $R\dot{O}_2$ can generate highly oxygenated organic molecules (HOMs), which increase secondary organic aerosol production thus promote new particle formation [1, 4-6]. In combustion, chain branching reactions initiated by peroxy radicals are at the heart of low-temperature chemistry [7,8]. These radicals are formed when a carbon-centered radical ($\dot{R}$) combines with O_2, and can react via a number of competing degradation pathways (Fig. 1). Macroscopic phenomena such as fuel auto-ignition, flame propagation, and atmospheric visibility depend on which of the many competing reactions dominates the fate of these $R\dot{O}_2$ species.

In combustion systems, degradation of $R\dot{O}_2$ is dominated by intramolecular hydrogen migration to a carbon-centered hydroperoxyalkyl radical (QOOH), which can undergo β-scission yielding a reactive $\dot{O}H$ and therefore plays an important role in radical chain propagation. In contrast, unimolecular reactions of $R\dot{O}_2$ in the atmosphere assumed to be too slow, and thus these radicals are assumed to degrade primarily via bimolecular reaction with NOx, $\dot{O}H$, $H\dot{O}_2$ and other $R\dot{O}_2$ species [9,10]. However, the importance in the isomerization of $R\dot{O}_2$ arises from the formation of highly oxygenated organic molecules (HOMs), which greatly contribute to the formation and growth of atmospheric particles [1,4-6]. It means that the $R\dot{O}_2$ chemistry known to occur in one regime cannot be discounted in the other [11–13].

Here, focus is placed on the simplest ether, dimethyl ether (DME), which is considered an attractive alternative and/or a fuel additive due to its high octane number (CN $\geq$ 55), low gaseous and particulate emissions [14]. Upon the extensive usages, it can enter the atmosphere, where it is oxidized and affect the air quality [15,16]. It is therefore important to understand the chemistry of $R\dot{O}_2$ in DME under a wide condition, which spans the typical range of atmospheric and combustion conditions. Despite this awareness of the importance of $R\dot{O}_2$ intermediates, its branching ratio (i.e., the percentage of reaction channels generating RO_2 or producing $\dot{O}H$ in the $CH_3O\dot{C}H_2 + O_2$ reaction) and the temperature-/pressure-dependent effects have eluded due to the limited experimental detection [17–24]. Therefore, experimental measurements combined with theory are essential to fill a gap in the knowledge of $CH_3OCH_2O\dot{O}$ chemistry.

In *this study*, with a combination of single reference and multi-reference electronic structure calculations, we conclusively determine the detailed potential energy surface (PES) of multichannel $CH_3O\dot{C}H_2$ + O_2 reactions, and with microcanonical variational transition state theory (μVT), 1-D tunneling approximation, multi-conformer and torsional potential contribution, corresponding temperature-/pressure-dependent rate coefficients are determined.

* Corresponding authors.
E-mail addresses: yjzhang_xjtu@xjtu.edu.cn (Y. Zhang), zhhuang@xjtu.edu.cn (Z. Huang).

https://doi.org/10.1016/j.combustflame.2024.113339
Received 8 July 2023; Received in revised form 21 January 2024; Accepted 24 January 2024
Available online 7 February 2024
0010-2180/© 2024 The Combustion Institute. Published by Elsevier Inc. All rights reserved.

2. Theoretical and computational approach

2.1. Electronic structure calculations

Twenty stationary points were computed for the $CH_3O\dot{C}H_2 + O_2$ reaction potential energy surface (PES). For each species and transition state (TS), systematic conformer searches were carried out using the B3LYP method [25] with the 6-311+G(d,p) basis set [26,27]. The B3LYP method was chosen because its implementation is usually very efficient and it has been widely tested [28–30]. In addition, it has been found to accurately predict the energy ordering of conformers [31–33]. In a systematic conformer search, since the target reaction system involves only small molecules or radicals, the default setting of rotations (a factor of 3 for bonds composing of sp^3 hybridized atoms while a factor of 2 for bonds composing of sp^2 hybridized atoms) was assigned for each single bond. In the case for searching conformers of transition states, constrains were placed on bond lengths of "transition regime" (bonding and breaking) before the conformer search was initiated, as no conformer sampling algorithms for transition state structures were available [34]. Although transition state force fields (TSFFs) exists, it need to be parametrized specifically for the reaction studied [35,36].

The geometry of the lowest energy conformer was re-optimized for all the stationary points using the M06-2X method [37] with the Def2-TZVP basis set [38]. The M06-2X method [37] was adopted to obtain more accurate thermokinetic calculations due to its wide acceptance in the treatment of the main group thermochemical kinetics [39–43]. For step-by-step verification of the transition states (TSs), intrinsic reaction coordinate (IRC) calculations were used to identify saddle points connecting reactants and products at the same level of theory.

Coupled cluster theory CCSD(T)/cc-pVTZ and CCSD(T)/cc-pVQZ [44,45] energies were calculated using the density function theory (M06-2X/Def2-TZVP) geometries. The CCSD(T) complete basis set (CBS) limit was extrapolated from the triple and quadruple zeta basis set calculations assuming an inverse power law [46–48]

$$E_{CBS} = E_{QZ}^{CC} + \left(E_{QZ}^{CC} - E_{TZ}^{CC}\right) \times \frac{4^4}{5^4 - 4^4} \quad (1)$$

where the E_{CBS} is the energy extrapolated to CBS, and the *E*CC QZ and the ECC TZ means the calculated energies at the CCSD(T)/cc-pVQZ and the CCSD(T)/cc-pVTZ level respectively. The CCSD(T)/CBS enthalpies at 0 K, including the 0.971 scaled M06-2X zero point energies, for the $CH_3O\dot{C}H_2 + O_2$ PES are listed in Tables S5 and S6. Also included in these tables are the CCSD(T)/cc-pVTZ and CCSD(T)/cc-pVQZ T1 diagnostic for the equilibrium and saddle point geometries, which is a measure of the importance of multi-reference configuration interaction [49]. Single reference calculations are capable of treating the wave functions of the stationary points that possess the tiny T1 diagnostics. That is, T1 diagnostic values larger than 0.03 for radicals or 0.02 for closed shell species are often taken to be indicative of the possibility for significant multi-reference effects [50].

On the other hand, as the addition of molecular oxygen to a methoxymethyl radical proceeds without an intrinsic barrier, the multi-reference characteristic is crucial in describing such processes. Figures S2 and S3 compared the present calculated points of potential curve for the target reaction $CH_3O\dot{C}H_2 + O_2 \rightarrow CH_3OCH_2O\dot{O}$ at various levels of theory. On this basis, second-order multi-reference perturbation theory (CASPT2) with aug-cc-pVTZ basis set [51–54] optimizations were performed along the minimum energy path (MEP) from 1.6 to 6.0 Å. It is well known that the size of the active space directly affects the accuracy of the calculation results. In general, the larger the active space is the more accurate the calculation results will be, but it is often more computationally expensive. In order to give consideration to the requirements of accuracy and computational cost, the active space of (7e, 5o) was selected, specifically six electrons in four orbitals for molecular oxygen and one electron in one orbital for the carbon-centered radical [55–57]. All single reference calculations were performed using Gaussian 09 [58] and CASPT2 calculations were done using MOLPRO version 2019.2 [59–61].

2.2. Kinetics calculations

The Rice-Ramsperger-Kassel-Marcus (RRKM)/Master Equation (ME) method [62] was employed to compute the temperature- and pressure-dependent rate coefficients. For the calculation of pressure-dependent rate coefficients, the chemically significant eigenstate approach proposed by Klippenstein and Miller [63,64] provides the basis for relating the eigenstates of the transition matrix to the phenomenological rate coefficients. The pressure-dependent rate coefficients were determined by solving the time-dependent multiwell master equation, which is usually written as:

$$\frac{d|w(t)\rangle}{dt} = G|w(t)\rangle \quad (2)$$

where the Hermitian matrix G describes chemical exchanges between different well and products, as well as collisional energy transfer in each well. $|w(t)\rangle$ is a vector containing populations of energy states in all the wells at time t [63–65]. To account for the weak temperature- and size-dependence of the energy transfer parameter, $\langle\Delta E_{down}\rangle$ ($200\times(T/300)^{0.85}$ cm^{-1}) [66] was used for the $CH_3O\dot{C}H_2 + O_2$ reaction PES. The collision frequency was estimated using a Lennard-Jones (L-J) model, with L-J parameters of σ = 4.36 Å and ε =292 cm^{-1} for $CH_3OCH_2O\dot{O}$, and σ = 3.6 Å, ε = 68 cm^{-1} for N_2 as the bath gas. The L-J parameters refer to those from the $C_3H_7O_2$ system studied by Goldsmith et al. [66]. For each requested temperature and pressure the global relaxation matrix was constructed by appropriate discretization, the chemically significant eigenstates were used to evaluate all of the phenomenological rate coefficients.

The barrier-less process was treated by microcanonical variational transition state theory (μVT) [67], while reactions with intrinsic barrier were treated with conventional transition state theory (TST) [68] employing RRHO assumptions for most modes. More details on the description of the microcanonical variational treatment of the barrier-less channel of CH_3OCH_2 plus O_2 are provided as the **Supporting**

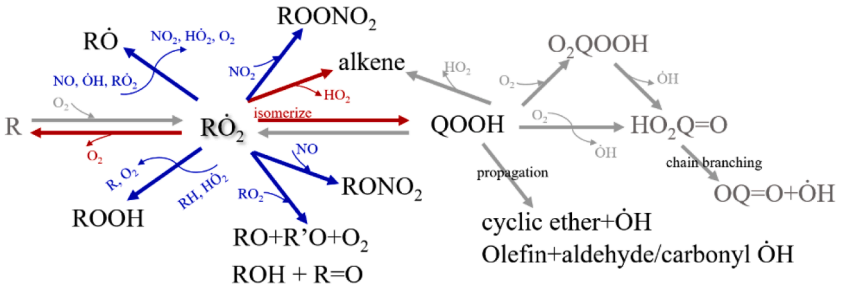

Fig. 1. Unimolecular (red)/bimolecular (blue) reactions of $R\dot{O}_2$, and chain reactions (gray) initiated by these radicals.

Information (S1.2 and S2.1). Considering anharmonicity of the target system and the systematic error caused by the theoretical method, an F scale factor of 0.946 was adopted to correct the vibrational frequencies. This treatment results in comparable frequencies between the theoretical calculations and experimental measurements [69]. For low frequency vibrational modes corresponding to the rotation of a single bond, 1-D hindered rotor approximation were used to describe the torsional modes. For the tunneling coefficient, the widely employed 1-D Eckart approach [70] was used in *this study*. All 1-D master equation calculations were performed using the PAPR solver at pressures of 0.01 – 100 atm over the temperature range of 298.15 – 1200 K. Since the current modification of the PAPR solver [71] to the direct diagonalization method incorporate key elements of the low eigenvalue method for cases where the span of eigenvalues is too large, the direct diagonalization method was selected in the calculation of the PAPR master equation code [71]. Note that in the PAPR input, μVT calculations were performed by using the "Variational" keyword, which represents a variational approach to the evaluation of the transition state number of states.

3. Results and discussion

3.1. Potential energy surface

Due to the special C—O-C—O-O backbone structure of $CH_3OCH_2O\dot{O}$ radical, yielding an alkene and $H\dot{O}_2$ radical is not possible as there is no abstractable H-atom on the central oxygen atom. The absence of this reaction type has important impact on the fuel reactivity in the low-temperature regime. Fig. 2 shows the zero-point corrected PES for $CH_3O\dot{C}H_2 + O_2$ reactions. The relative energies for the minima and saddle points on this PES are listed in Supporting Information (Table S5 and Table S6, respectively).

The $CH_3OCH_2O\dot{O}$ radical is formed from $CH_3O\dot{C}H_2 + O_2$, which proceeded without an intervening potential energy barrier (Figure. S5). Systematic conformer searches were carried out at the B3LYP/6-311+g (d,p) level, and the optimized conformers with an electronic energy (E_e) difference larger than 2 kcal•mol^{-1} and/or Boltzmann distributions smaller than 0.05 were removed. The following is to re-optimize the retained conformers at the M06-2X/Def2-TZVP level. The M06-2X optimized conformers with E_e difference smaller than 1×10^{-5} Hartree and a dipole moment difference smaller than 1.5×10^{-2} Debye were regarded as identical conformers, and duplicates were removed [34]. Four unique conformers of $CH_3OCH_2O\dot{O}$ were identified (Figure. S6).

It is well established that isomerization of $CH_3OCH_2O\dot{O}$ to a carbon-centered hydroperoxy-methyl-methoxy radical ($\dot{C}H_2OCH_2O_2H$) can occur *via* intramolecular hydrogen migration. The 1,3 H-shift reaction of $CH_3OCH_2O\dot{O}$ can generate the $CH_3O\dot{C}HOOH$ radical, but the formed $CH_3O\dot{C}HOOH$ is unstable and immediately decomposes to P1, CH_3O-CHO + ȮH (Figure. S7). However, this reaction pathway is rather difficult due to the significant barrier ($TS_{H\text{-}shift}2$). In contrast, the 1,5 H-shift reaction through a six-member ring TS ($TS_{H\text{-}shift}1$) shows greater dominance. The formed $\dot{C}H_2OCH_2O_2H$ has conformers (Figure. S8) analogous to those for $CH_3OCH_2O\dot{O}$, however, the O—OH bond in the former allows for more minima, as rotation about the O—O bond is hindered (Figure. S9).

Decomposition of $\dot{C}H_2OCH_2O_2H$ into two formaldehyde molecules (CH_2O) and a hydroxyl radical (ȮH) completes the propagation path. This reaction channel also be regarded as the dominant reaction pathway *via* the fission of $\dot{C}H_2OCH_2O_2H$ in previous theoretical studies [20,75-77]. Two transition states for $\dot{C}H_2OCH_2O_2H$ dissociate into $2CH_2O$ + ȮH (P2), $TS_{dec}1$ and $TS_{dec}1$', were found in *this study*. The transition state, denoted by $TS_{dec}1$, possesses lower energy with respect to the entrance energy of $CH_3O\dot{C}H_2 + O_2$. This transition state involves first a scission of O—O bond, forming CH_2OCH_2O fragment and ȮH fragment, the resulting CH_2OCH_2O is unstable and rapidly dissociates into two formaldehyde molecules. For $TS_{dec}1$', another transition state connecting $\dot{C}H_2OCH_2O_2H$ and products $2CH_2O$ + ȮH, it is higher in energy than $TS_{dec}1$. In this transition state, the C—O bond in $\dot{C}H_2O$—CH_2O_2H radical breaks first, and the resulting $\dot{C}H_2O_2H$ fragment is not stable and readily dissociates into one formaldehyde molecule and one hydroxyl radical. It makes considerable sense that the reaction barrier to break an O—O bond should be weaker than one to break a C—O bond. The reason is that lone pair-lone pair repulsion between these two oxygen weakens the O—O bond relative the C—O bond,

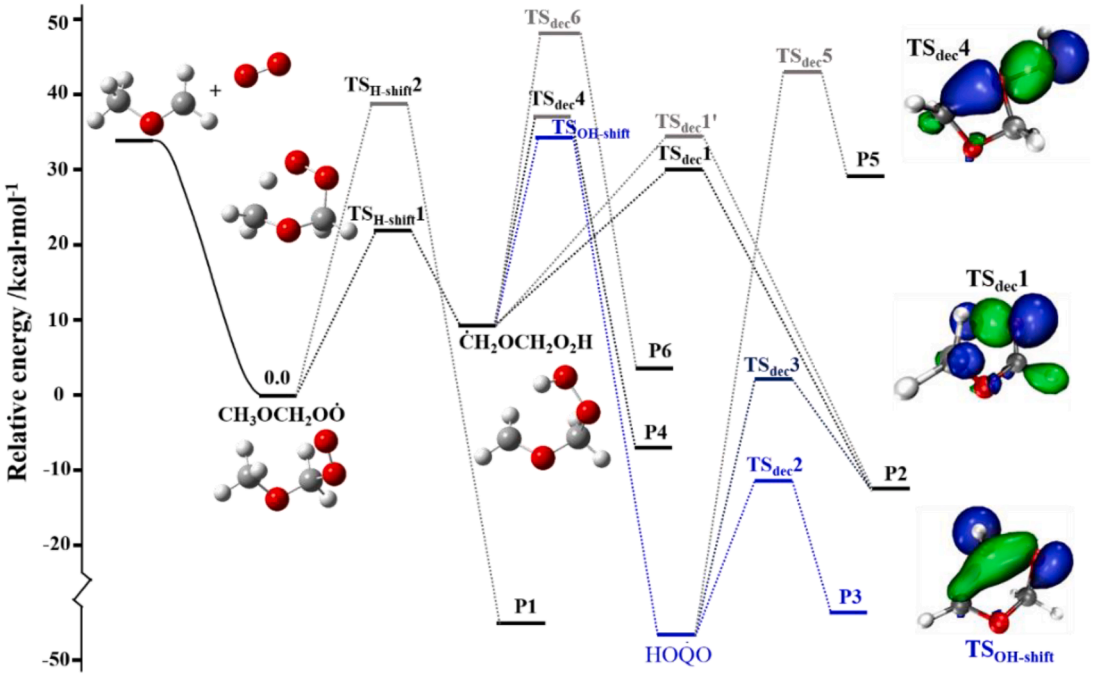

Fig. 2. Energy diagram for the fate of $CH_3OCH_2O\dot{O}$ radical. The relative energy of $TS_{dec}1$, $TS_{OH\text{-}shift}$, and $TS_{dec}4$ were determined by multi-reference methods (more details are provided in the SI), and orbital isosurfaces were plotted by Multiwfn 3.8 [72,73] and VMD 1.9.3 [74]. HOQO means $HOCH_2OCH_2O$.

resulting in a lower barrier.

Considering that both of $TS_{dec}1$ (T1 = 0.059 for the CCSD(T)/cc-pVTZ level and 0.052 for the CCSD(T)/cc-pVQZ level) and $TS_{dec}1$' (T1 = 0.031, 0.031) show strong static correlation due to the T1 diagnostics are over the thresholds for concern (T1 > 0.03), the MRCI//CASPT2 calculations were further employed for these two TSs and the intermediate ($\dot{C}H_2OCH_2O_2H$) to which they are connected. Optimization and frequency analysis of $\dot{C}H_2OCH_2O_2H$ and $TS_{dec}1$ were finally optimized at the CASPT2 (7e,5o)/aug-cc-pVDZ level. The active space of (7e,5o) contains the σ and σ* orbitals for the breaking O—O bond ($HO\bullet\bullet\bullet OCH_2O\dot{C}H_2$), lone pair orbital of each oxygen atom for the O—O bond, and one electron in one orbital for the carbon-centered radical. The MRCI energy calculations were performed at the CASPT2 optimized geometry. Optimization for $TS_{dec}1$' geometry was carried out at the CASPT2 (3e,3o)/aug-cc-pVDZ level. The active space of (3e,3o) contains the σ and σ* orbitals for the breaking C—O bond ($HOOCH_2\bullet\bullet\bullet O\dot{C}H_2$) and one electron in one orbital for the carbon-centered radical. The result shows that the ground state of $TS_{dec}1$' (with the configuration interaction (CI) vector of 0.962 computed by MOLPRO) accounts for about 92.5 %, and its T1 diagnostic (0.031) is only slightly above the threshold of concern (0.03). This means that the influence of multi-reference can be ignored, and the single-reference method is acceptable. Therefore, in plotting the PES shown in Fig. 2 and in the subsequent kinetic calculations, the relative energy of $TS_{dec}1$ is derived from the multi-reference calculations while the relative energy of $TS_{dec}1$' is retain from the CCSD(T) calculations.

On the other hand, $\dot{C}H_2OCH_2O_2H$ may rearrange and decompose via $TS_{dec}4$ into 1,3-dioxetane and hydroxyl radical (P4), or, there are also two other possible channels that $\dot{C}H_2OCH_2O_2H$ could follow in rearranging or decomposing into products. One is $\dot{C}H_2OCH_2O_2H$ connects to ethylene oxide + $H\dot{O}_2$ (P6) via $TS_{dec}6$, and the other is $\dot{C}H_2OCH_2O_2H$ undergoes intramolecular –OH group migration to form $HOQ\dot{O}$ ($HOCH_2OCH_2\dot{O}$), which then connects to 1,2,4-trioxolane + H (P5) via $TS_{dec}5$. However, the barrier heights of $TS_{dec}5$ and $TS_{dec}6$ are entirely over the entrance energy of $CH_3O\dot{C}H_2 + O_2$. Therefore, these two channels are the least favorable pathways for $CH_3O\dot{C}H_2 + O_2$ to follow.

Similar to the case of $TS_{dec}1$ and $TS_{dec}1$', the transition state $TS_{dec}4$, possessing a higher T1 diagnostic (0.038 for the CCSD(T)/cc-pVTZ level and 0.039 for the CCSD(T)/cc-pVQZ level), shows a strong static interaction. Considering that $TS_{dec}4$ describes the fission of O—OH bond and the bonding of terminal C atom and O atom, geometry of $\dot{C}H_2OCH_2O_2H$ and $TS_{dec}4$ were optimized at the CASPT2 (7e,5o)/aug-cc-pVDZ level. Since $TS_{dec}4$ describes the trend of O—O fission following by C—O bonding, the active space of seven electrons in five orbitals was chosen. It consists of one electron in one orbital for the carbon-centered radical, the bonding and antibonding orbital of O—O bond, and lone pair orbital of each oxygen atom for the O—OH bond. Frequency analysis and the MRCI energy calculations were performed at the CASPT2 optimized geometry. Again, the reaction barrier of $TS_{dec}4$ (i.e., the relative energy provide in Tables S6) in Fig. 2 is the energy calculated at the MRCI method.

In addition, $\dot{C}H_2OCH_2O_2H$ also appears to be able to undergo an OH migration to form $HOCH_2OCH_2\dot{O}$ ($HOQ\dot{O}$), following by rearranging and decomposing to generate $2CH_2O + \dot{O}H$ (P2) and $H\dot{C}O + H_2O +$ CH2O (P3) via $TS_{dec}3$ and $TS_{dec}2$ respectively. For the product channel of generating P3, Suzaki et al. [20] first proposed this mechanism to reproduce the amount of $H\dot{O}_2$ through their experimental measurement. The barrier of OH migration in this study is 0.6 kcal•mol^{-1} above $CH_3O\dot{C}H_2 + O_2$, while the value reported by Suzaki et al. [20] is below $CH_3O\dot{C}H_2 + O_2$. The CASSCF calculation adopted by Suzaki et al. can well describe static interaction, but it cannot accurately describe the dynamic correlation. Moreover, considering the theoretical methods involved in this study are completely different from that of Suzaki et al., it is indeed difficult to directly compare the differences between the reaction barriers.

Since the T1 diagnostic values for TS_{OH_shift} (0.061 for calculation at the CCSD(T)/cc-pVTZ level and 0.053 for calculation at the CCSD(T)/cc-pVQZ level) are above the thresholds for concern (T1 > 0.03), CASPT2 (7e,5o)/aug-cc-pVDZ calculation was performed to attain the geometry of the transition state ($TS_{OH\text{-}shift}$) of OH migration. The active space of (7e,5o) consist of the highest singly occupied molecular orbital, the bonding and antibonding orbital of O—O bond, and lone pair orbital of each oxygen atom of O—OH bond. Frequency analysis was performed at the same level of theory for the CASPT2 optimized geometry. Furthermore, the MRCI energy calculation were performed for the CASPT2 optimized $TS_{OH\text{-}shift}$ geometry. In order to calculate the MRCI reaction barrier, the single-point energy of QOOH was calculated at the MRCI/aug-cc-pVDZ// CASPT2 (7e,5o)/aug-cc-pVDZ level of theory.

The formed $HOCH_2OCH_2\dot{O}$ undergoes rearrangement and decomposition to generate $2CH_2O + \dot{O}H$ via $TS_{dec}3$ and $H\dot{C}O + H_2O + CH_2O$ via $TS_{dec}2$, respectively. $TS_{dec}3$ is a looser transition state than $TS_{dec}2$ and possesses a higher value of T1 diagnostic (T1 = 0.032). Geometry of $HOCH_2OCH_2\dot{O}$ and $TS_{dec}3$ were finally optimized at the CASPT2 (13e,11o)/aug-cc-pVDZ level. This active space consists of the highest singly occupied molecular orbital, the bonding and antibonding orbital of each C—O bond, and lone pair orbital of each oxygen atom. As in the case of $TS_{dec}1$', the T1 diagnostic of $TS_{dec}3$ (0.032) is slightly above the threshold of 0.03, and the ground state of $TS_{dec}3$ accounts for about 94.2 % due to 0.970 of CI vector. It seems that the influence of multi-reference can be ignored, and the single-reference result is acceptable.

3.2. Torsional modes calculation

The torsional modes play a significant role in calculating density of states through the Laplace transform of the partition function. For rotations of each single bond of stationary points present in Fig. 2, the rotational PES were calculated by a relaxed scan at the M06-2X/Def2-TZVP level of theory. The internal rotational PES of $CH_3OCH_2O\dot{O}$ is displayed here for instance, Fig. 3. In general, if the barrier to internal rotation is ≈ 2R*T* (the thermal energy) or greater than that at the highest temperature of interest, it is likely safe to treat the degree of freedom using the vibrational partition function without a loss of accuracy in the computed thermodynamic or kinetic functions. In other word, if the rotational barrier is lower than thermal energy (2R*T*, $T \geq 298$ K), this barrier can be overcome, it is then better to treat this low-frequency vibrational mode with 1-D hindered rotor. Therefore, the vibrational modes corresponding to the CH_3—$OCH_2O\dot{O}$ and CH_3OCH_2—$O\dot{O}$ bonds are described by 1-D hindered rotor in kinetics calculation.

As introduced above, in the calculation process of *this study*, the Rigid-Rotor Harmonic-Oscillator (RRHO) model was adopted except for the vibrational modes that correspond to low-frequency torsional motions. These low-frequency torsional motions in calculating partition functions were treated as the one-dimensional hindered rotor (1-DHR). In order to more visually show the impact of the 1-DHR treatment on the calculated rate coefficients, Fig. 4 compares the calculations including 1-D HR treatment (solid lines) with that calculating only by Rigid-Rotor Harmonic-Oscillator (RRHO) model (dashed lines). Moreover, the MC-TST calculated rate coefficient of $CH_3OCH_2O\dot{O} \rightarrow \dot{C}H_2OCH_2O_2H$ reaction (at 298 K) from Kristian et al. [10] is also plotted in Fig. 4 for comparison. In the studied temperature range, the hindered rotor effect can influence the rate coefficient by factors of 2.7–3.0, 3.2–8.3 and 4.0–6.6 for the addition, isomerization and decomposition, respectively. It's clearly that the discrepancy appears to be more prominent with increasing temperature. It is no surprise because the RRHO model performs well at lower temperatures but it cannot accurately describe the vibrational potential at higher temperatures.

3.3. Quantum mechanical tunneling effect

Considering quantum-mechanical tunneling has a great contribution to chemical rate coefficients at low temperature, especially for reactions involving the low mass of the hydrogen atom being transferred [78].

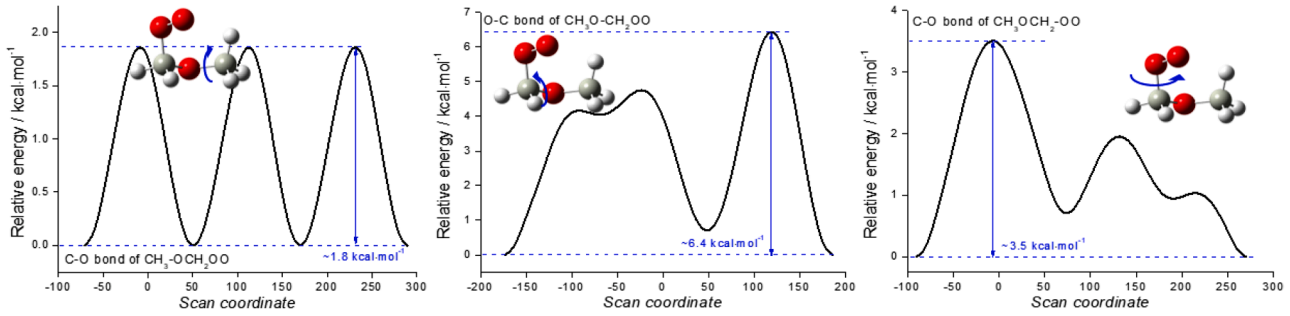

Fig. 3. Rotational PES of $CH_3OCH_2O\dot{O}$ radical. From the left are R-CH_3 group, CH_3O-R group and R-OO group.

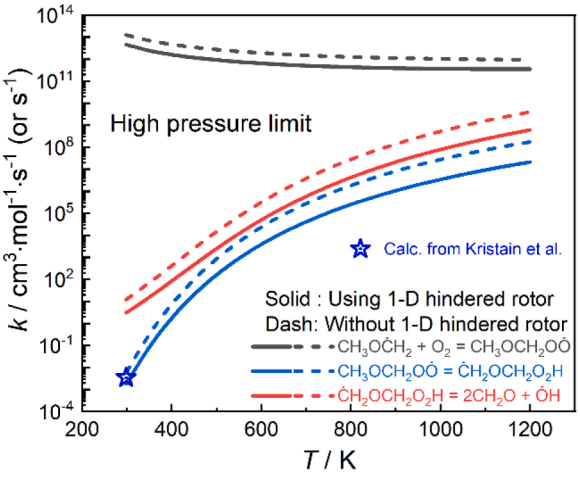

Fig. 4. Effect of internal rotors on calculated rate coefficients.

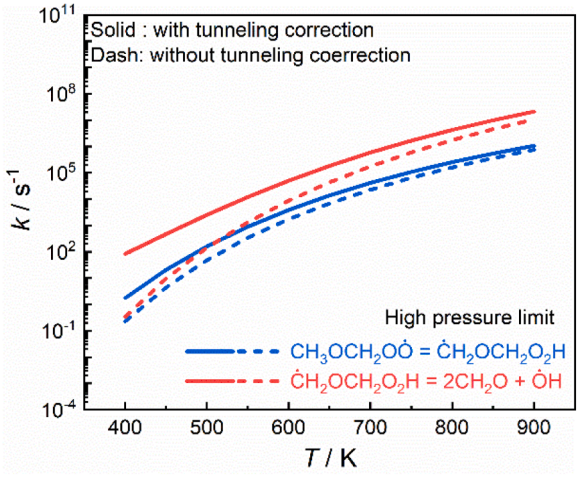

Fig. 5. Influence of quantum mechanical tunneling effect on calculated rate coefficients.

Chemical reaction rate coefficients of reactions with intrinsic barrier were calculated using TST including quantum-chemical tunneling. In TST, the reaction rate coefficient (k) is given by:

$$k = \kappa \frac{k_B T}{h} \frac{Q_{TS}}{Q_R} \exp\left(-\frac{E_{TS} - E_R}{k_B T}\right) \quad (3)$$

Where κ is the quantum-mechanical tunneling coefficient, k_B is Boltzmann's constant, T is the absolute temperature, h is Plank's constant, Q_{TS} and Q_R are the total partition functions of the transition state and reactants, respectively. The difference in energy between the reactants and transition state is the reaction barrier.

Here, the widely employed 1-D Eckart approach [70] was used to calculate the tunneling coefficient κ. Eckart tunneling is a simple one-dimensional tunneling approach in which the tunneling coefficient is calculated by solving the Schrödinger equation for an asymmetrical one-dimensional Eckart potential. It is the exact solution to an approximate potential derived from the barrier heights on both sides of the TS and its imaginary frequency.

The quantum mechanical tunneling effect for the main reaction sequence was plotted here for instance (Fig. 5). As expected, the tunneling effect on the rate coefficients decreases and gradually converges as the temperature increases. Specifically, with considering the tunnelling effect, the calculated rate coefficients can be increased by factors of 1.4–7.6 (900 – 400 K) and 2.0–248 (900 – 400 K) for the isomerization and decomposition, respectively.

3.4. Theoretically calculated rate coefficients

The present predicted rate band for $CH_3O\dot{C}H_2 + O_2$ →products (at 298.15 K and various pressures) are compared in Fig. 6 with the corresponding experimental measurements [17,19,21,24,79]. Where the

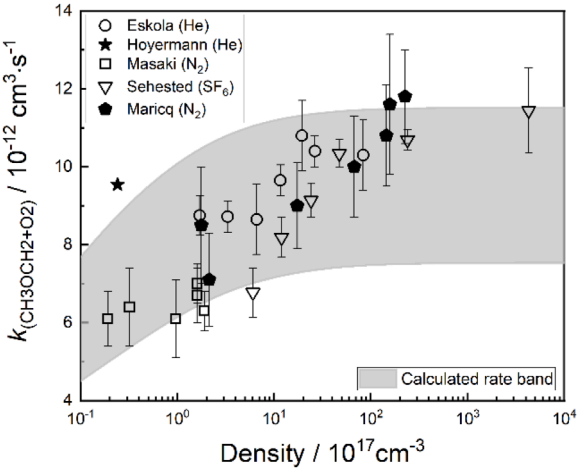

Fig. 6. Comparison of the present calculations with the experimental data available in literatures. The experimental data correspond more or less to a temperature of 298 K.

gray shadow represents the calculated uncertainty of rate coefficient for the $CH_3O\dot{C}H_2 + O_2$ reaction. The experimental data shown in Fig. 6 correspond more or less to a temperature of 298 K.

In particular, for this calculated rate band, it is obtained by taking into account the uncertainty from the energy, frequency and collisional parameters at each point of this barrier-less reaction process (A brief discussion about the uncertainty estimation was provided in the **Supporting Information**). With a combination of the above factors (energy,

frequency and collision parameters), there is a difference ranging from 1.7 to 1.5 times between the calculated upper limit and lower limit as the pressure increases. The experimental data almost lie within the calculated rate band of *this study*, implying that the present calculations are generally in reasonable agreement with the experimental data with considering the experimental uncertainty. It thus verifies the reliability of the theoretical rate coefficients calculated in *this study*.

With reference to saturated straight-chain alkanes system, depending upon the temperature and pressure, the reactants ($CH_3O\dot{C}H_2 + O_2$) can proceed directly to the various product channels on the same time scale as collisions without first being stabilized into the peroxy radical. Similarly, the individual $CH_3OCH_2O\dot{O}$ and $\dot{C}H_2OCH_2O_2H$ isomers can decompose across multiple transition states directly to nonadjacent products. These well-skipping pathways are an essential component of the $CH_3O\dot{C}H_2 + O_2$ reaction system, and quantitative description of the temperature- and pressure-dependent rate coefficients can be obtained from the eigenvalue solution to the master equation (Table S9). In order to test the well-skipping that could be described by the PES constructed in *this study*, Fig. 7 is plotted to compare the theoretical ȮH yield with the experimental one at 295 and 450 K. Although the theoretical calculation tends to slightly under-estimate the experimental measurements, in general, such errors are acceptable.

On the other hand, considering that the input parameter involved in RRKM/ME calculations can be divided into three categories: energy, frequency and collisional parameters. Therefore, the combined influence of these three aspects as well as the low-frequency torsional motions on calculations is also considered. The uncertainty of the input parameters for kinetic calculations are provided in Table S4. The complete set of temperature-/pressure-dependent rate coefficients (as well as the computational uncertainty) for the calculated $CH_3O\dot{C}H_2 + O_2$ reactions are provided as a CHEMKIN-compatible PLOG format with modified Arrhenius parameters (Tables S7 – S10).

The calculated high-pressure limit (HPL) rate coefficients of the entrance channel for $CH_3O\dot{C}H_2 + O_2$ reaction are compared in Fig. 8 with that used in literature models [77,80-86], as well as the theoretical calculations [20,75,76]. Even considering the computational uncertainty, most of literature recommendations deviate from the computational error band especially at higher temperatures ($T > 450$ K). This is perhaps due to an incomplete picture of the bond-breaking process. Since there is a fact that the theoretical researches from Andersen [75] and Yamada et al. [76] were performed at the B3LYP/6-311G** level and the CBS-q//MP2(full)/6-31G** respectively.

The B3LYP method (~20 % Hartree-Fock exchange) [25] has limited

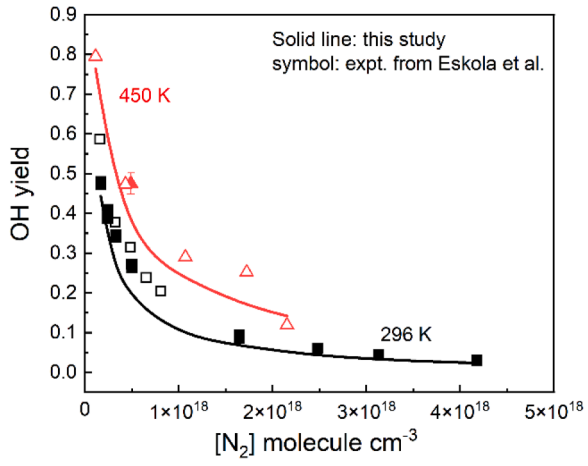

Fig. 7. Comparison between experimental and theoretical ȮH yields of $CH_3O\dot{C}H_2 + O_2$ reaction versus [N_2] at 296 and 450 K. The solid lines correspond to master equation calculations of this study, while the symbols mean the experimental data provided by Eskola et al. [22].

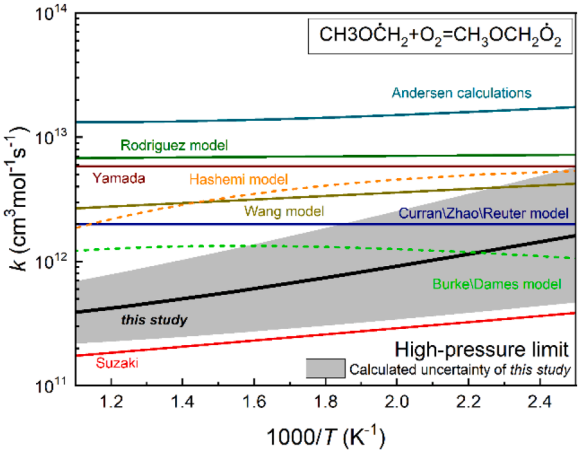

Fig. 8. Comparison of HPL rate coefficient for $CH_3O\dot{C}H_2 + O_2 \rightarrow CH_3OCH_2O\dot{O}$ reaction channel. The data used in the Hashemi model were obtained by fitting the chebyshev polynomial provided by Eskola et al. [22].

ability to deal with the current system with strong static correlation. The CBS-q method (and variants) have "special problems" with (population) localization in molecules having multiple lone pairs on the same atom, spin contamination, and molecules with symmetry. That is, the CBS-q method may be expected to have particular problems with peroxy radicals, where two of the three features mentioned above are present.

The RRKM/ME calculations for $CH_3O\dot{C}H_2 + O_2$ are plotted in Fig. 9. For simplicity, the discussion will be limited to the result at 1 atm (other pressures are provided as Figure. S12).

The dominant product channel is generating $CH_3OCH_2O\dot{O}$ at temperature below 1250 K. The rate coefficients of $\dot{C}H_2OCH_2O_2H$ and $2CH_2O + \dot{O}H$ are 2 and 4 orders of magnitude smaller than $CH_3OCH_2O\dot{O}$ ones at 298 K, respectively. As the temperature increases, the rate coefficients of association reaction generating $CH_3OCH_2O\dot{O}$ and well-skipping channel producing $\dot{C}H_2OCH_2O_2H$ decrease, while the chemically activated reaction resulting in $2CH_2O + \dot{O}H$ increases. This behavior is roughly similar at the other pressures (Figure. S12). However, the temperature of branching ratio changeover decreases as the pressure decreases, and thus we believe that pressure-dependent rate coefficients are still needed to accurately describe the competition of association and well-skipping reactions.

On the other hand, the rate coefficients for the directly $H\dot{C}O + CH_2O + H_2O$ generation are 5 orders of magnitude smaller than $CH_3OCH_2O\dot{O}$ one at 400 K and a factor about 65 smaller than that of $CH_3OCH_2O\dot{O}$ at 1450 K, respectively. It shows that the three-products channel do not appear to be favorable.

For the isomerization reaction ($CH_3OCH_2O\dot{O} \rightarrow \dot{C}H_2OCH_2OOH$), as Andersen et al. [75] have reported, the pressure dependence of the present calculated rate coefficient ($p \geq 1$ atm) can be negligible. In practice, the present calculated rate coefficients at 1 atm are 2–3 times different from high-pressure limit rate coefficients at 850 – 1000 K (Fig. 10), which is beyond the calculated uncertainty about a factor of 1.5 (Tables S9 and S10). Note that the rate coefficient of isomerization under atmospheric condition is 99 % close to the HPL value (Figure. S13). At lower pressures however, the rate coefficient deviates more significantly from the HPL as the temperature increases.

This phenomenon is consistent with the pressure-dependent rate coefficients usded in the Hashemi model [86]. Note that the data used in the Hashemi model were obtained by fitting the the chebyshev polynomial provided by Eskola et al.[22], see Figure. S14. However, Rodriguez et al. [77] predicted the fastest isomerization rate coefficients based on the G4 level energies, which are about five times faster than the present calculations. The recommendation from Yamada et al. [76] is ~2.5 times faster than the present calculation at 1000 K, while the deviation between Yamada et al. recommendation and the present

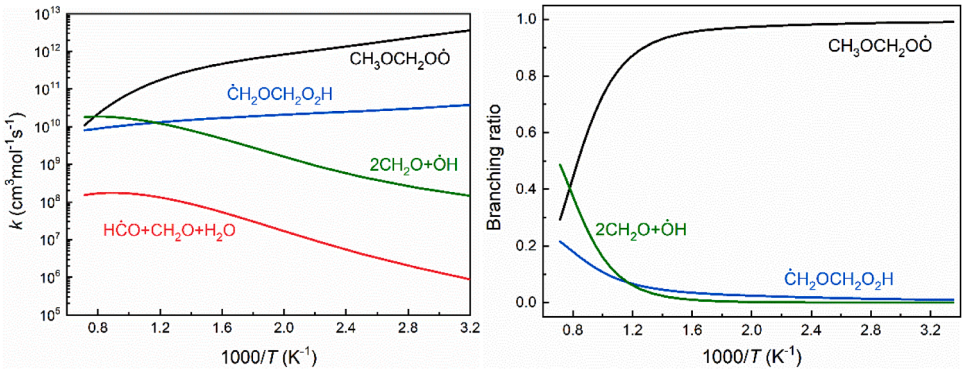

Fig. 9. RRKM/ME rate coefficient (left) and branching ratio (right) for $CH_3O\dot{C}H_2 + O_2$ reactions at 1 atm.

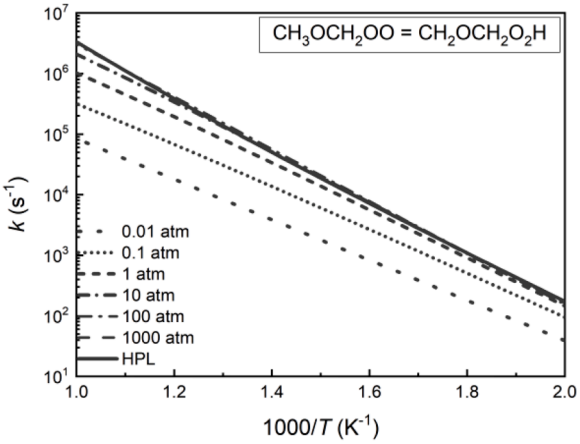

Fig. 10. RRKM/ME calculated pressure-dependent rate coefficients for isomerization from $CH_3OCH_2O\dot{O}$ to $\dot{C}H_2OCH_2O_2H$.

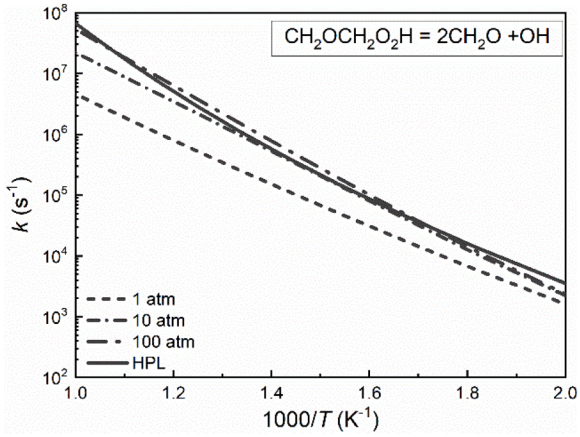

Fig. 11. RRKM/ME calculated pressure-dependent rate coefficients for decomposition reaction from $\dot{C}H_2OCH_2O_2H$ to $2CH_2O + \dot{O}H$.

calculation at 500 K is about 5 times (Figure. S15). In the investigation of Yamada et al.[76], the activation energy of H-shift isomerization TS is estimated from the reactant ($CH_3OCH_2O\dot{O}$) and product (CH_2O-CH_2O_2H). Andersen and Carter [87] under-predicted the rate coefficients in the temperature range below ~775 K, however, over-predicted the rate coefficients in the temperature range above ~775 K. The lack of "special treatment", such as hindered rotor for lower frequency vibrational modes from harmonic oscillators and quantum-chemical tunneling, increases the uncertainty of their calculations.

For the $\dot{C}H_2OCH_2OOH$ decomposition, a pressure-dependent behavior of the currently calculated rate coefficients can be observed from Fig. 11. There is a deviation between the rate coefficients at various pressures, and this difference becomes more significant with decreasing pressure and increasing temperature. For instance, at a pressure of 1 atm, the difference between the rate coefficient and the HPL is within a factor of 2.2 at 500 K, however, as the temperature increases to 1000 K, the difference is up to a factor of 14.5. This implies that it is challenging to accurately predict the combustion behavior of DME at various pressures if only HPL is used to describe the decomposition kinetics of $\dot{C}H_2OCH_2OOH$.

The comparison result shows that Andersen and Carter [87] appear to over-predicted the HPL rate coefficient. At 298.15 K, the HPL provided by Andersen and Carter [87] is about 81,900 times faster than the present calculated HPL, and at a temperature of 1200 K the HPL given by Andersen and Carter is about 740 times faster than the calculation of *this study*, Figure. S16. The possible reasons are as follows: 1) lacking of treatment for lower frequency vibrational modes; 2) quantum-chemical tunneling effect; 3) the potential of multi-reference character of the TS for $\dot{C}H_2OCH_2OOH$ decomposition has not been noticed. Yamada et al. [76] also provided the excessively fast HPL rate coefficient, as well as the recommendations ($360 < T < 820$ K) from the SI (Table S25) of Eskola et al.[22]. For Yamada et al. [76], they had to decrease their activation energy about 20 kJ•mol^{-1} to get good agreement with experiment in their QRRK calculations. For Eskola et al. [22], their recommendations (300 – 1000 K and 0.004 – 1362.551 atm) were extrapolated from the experimental results (195 – 650 K and 0.004 – 0.667 atm) using ab initio (CBS-GB3)/master equation calculations. The reliability of adjusting calculated active energy or extrapolating rate coefficient according to experimental results is unknown.

3.5. *Implications for DME kinetic mechanism*

The present calculations were incorporated into four DME mechanisms, the Burke model [82], the Wang model [83], the Reuter model [85] and the Dames model [84] to investigate effect of new $CH_3O\dot{C}H_2 + O_2 \rightarrow CH_3OCH_2O\dot{O}$ kinetics on model performance. Simulations were performed by CHEMKIN-PRO[88] using Closed Homogeneous Reactor. To explore whether the new $CH_3O\dot{C}H_2 + O_2$ kinetics have an impact on model performance in terms of predicting combustion macro phenomena (e.g. ignition delay times), the original and updated models were used to predict the auto-ignition of DME at two pressures (3 atm and 39.47 atm), Fig. 12.

In the case of lower pressure (3 atm), the new $CH_3O\dot{C}H_2 + O_2 \rightarrow CH_3OCH_2O\dot{O}$ kinetics results in a longer ignition delay in the negative temperature coefficient (NTC) region as well as at temperatures slightly below the NTC region, when compared with the original models. About two times differences in predicted ignition delay times was observed

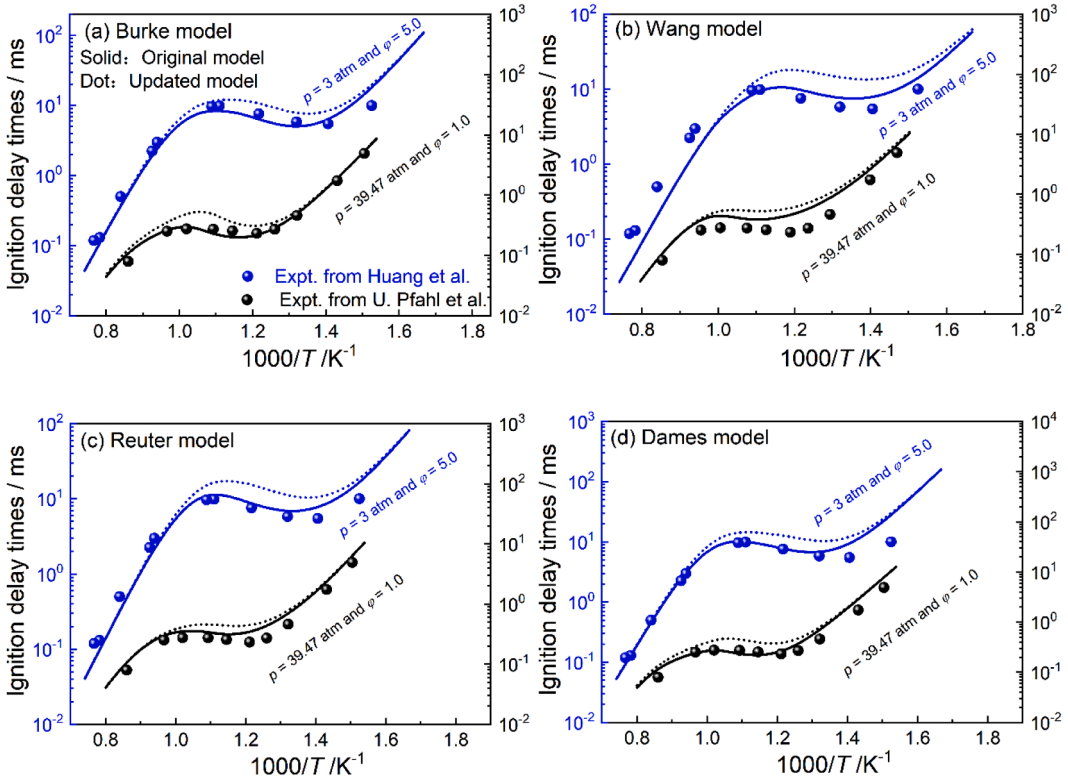

Fig. 12. Influence of new calculation of $CH_3O\dot{C}H_2 + O_2 \rightarrow CH_3OCH_2O\dot{O}$ kinetics on IDT for DME in "air" at different conditions. Blue line: fuel-rich (φ = 5.0) mixtures at 3 atm over the temperature range of 600 – 1350 K; black line: stoichiometric mixture at 39.47 atm over the temperature range of 650 – 1250 K. Symbols: Experiments, lines: model simulations with Burke model (a), Wang model (b), Reuter model (c) and Dames model (d).

before and after incorporating the current calculations. In contrast, the inclusion of the new $CH_3O\dot{C}H_2 + O_2$ kinetics has a limited effect on DME reactivity at temperatures higher than the NTC regime. It is no surprise because the kinetics of fuel radicals with molecular oxygen ($CH_3O\dot{C}H_2 + O_2$) governs auto-ignition features such as multistate ignition and NTC behavior at lower temperatures.

For the engine relevant condition (39.47 atm), the Burke model and the Dames model show the same sensitivity to the incorporating $CH_3O\dot{C}H_2 + O_2$ kinetics in terms of predicting ignition delay times. That is, the effect of new $CH_3O\dot{C}H_2 + O_2$ kinetics on the Burke model and the Dames model is mainly concentrated in the NTC region, whereas is has little effect in the high temperature region and limited effect in the low temperature region. For the Wang model and the Reuter model, although the main effect of the new $CH_3O\dot{C}H_2 + O_2$ kinetics is in the NTC region, the Wang model is also moderately affected in predicting high-temperature ignition of the DME after incorporating the new $CH_3O\dot{C}H_2 + O_2$ kinetics. It is not surprising because Dames et al. [84] retained the reactions corresponding to the first O_2 addition from the model of Burke et al. [82]. The $CH_3O\dot{C}H_2 + O_2$ kinetics has relatively limited effect on the Wang model and the Reuter model, while it results in an approximately two times deviation in the ignition delay predicted by the updated Burke model (as well as the Dames model).

In general, the effect of $CH_3OCH_2 + O_2$ kinetics on DME reactivity is mainly concentrated at NTC regime and temperatures below the NTC regime. This phenomenon can be well explained by the fact that IDT is essentially insensitive to the first O_2 addition reaction sequences at higher temperatures [82,85,86].

The above is for the impact of the entrance reaction channel of the first O_2 addition mechanism in DME low-temperature oxidation (i.e. $CH_3O\dot{C}H_2 + O_2 \rightarrow CH_3OCH_2O\dot{O}$) on the model performance, so does the updating of the $CH_3O\dot{C}H_2 + O_2$ reaction surface have any impact on the model performance? To further explore the effect of the first O_2 addition mechanism ($CH_3O\dot{C}H_2 + O_2$ reaction surface) of DME low-temperature oxidation on model performance, the key reaction channels shown in Table 1 were incorporated into the above four models to predict the auto-ignition of DME at 3 atm and 39.47 atm respectively (Fig. 13).

It is apparent that updating the kinetics of $CH_3O\dot{C}H_2 + O_2$ reaction surface has limited impact on the model performance in terms of predicting auto-ignition for the vast majority of the models tested in *this study*. That is, the simulation results for these four DME models are in reasonable agreement with the experimental measurements before and after incorporating the main reaction channels on the $CH_3O\dot{C}H_2 + O_2$ reaction surface listed in Table 1. This is in contrast to the aforementioned case where only the kinetics of the entrance channel of the first O_2 addition mechanism is updated. It follows that the satisfactory macroscopic performance of the existing kinetic models describing DME oxidation in reproducing the ignition delay times (IDTs) is due to the compensation of errors in the kinetic parameters of the $CH_3O\dot{C}H_2 + O_2$ reaction system. This may cause a cognitive illusion about the validity of the elementary reaction mechanisms.

It's not the authors' intention to judge the quality of a model's description of detailed chemistry, and it is out of the scope of the present paper to consolidate modeling efforts. However, the purpose of this study is to provide the theoretical kinetic parameters of $CH_3O\dot{C}H_2 + O_2$

Table 1
Reaction channels of $CH_3O\dot{C}H_2 + O_2$ kinetics incorporated into literature models.

No.	Reaction channel
1	$CH_3O\dot{C}H_2 + O_2 = CH_3OCH_2O\dot{O}$
2	$CH_3O\dot{C}H_2 + O_2 = \dot{C}H_2OCH_2O_2H$
3	$CH_3O\dot{C}H_2 + O_2 = 2CH_2O + \dot{O}H$
4	$CH_3OCH_2O\dot{O} = \dot{C}H_2OCH_2O_2H$
5	$CH_3OCH_2O\dot{O} = 2CH_2O + \dot{O}H$
6	$\dot{C}H_2OCH_2O_2H = 2CH_2O + \dot{O}H$
7	$CH_3O\dot{C}H_2 + O_2 = HCO + CH_2O + H_2O$

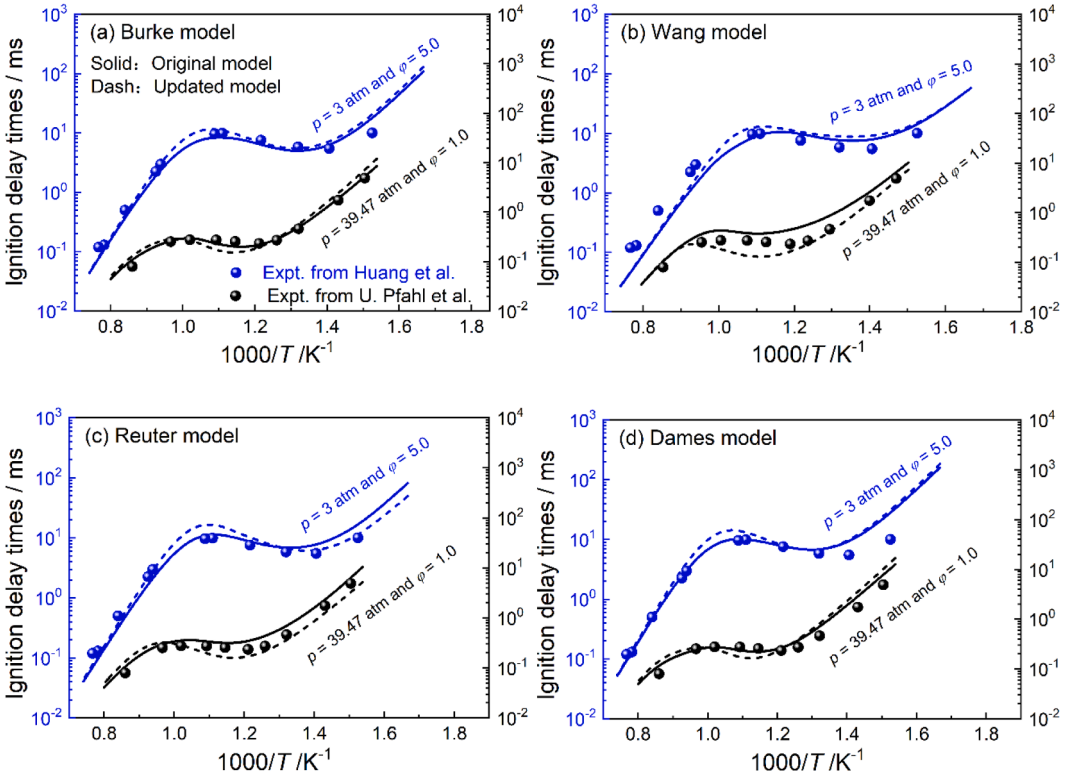

Fig. 13. Influence of the present calculated kinetics of $CH_3O\dot{C}H_2 + O_2$ reaction surface on IDT for DME in "air" at different conditions. Blue line: fuel-rich ($\varphi = 5.0$) mixtures at 3 atm over the temperature range of 600 – 1350 K; black line: stoichiometric mixture at 39.47 atm over the temperature range of 650 – 1250 K. Symbols: Experiments, lines: model simulations with Burke model (a), Wang model (b), Reuter model (c) and Dames model (d).

reactions and to verify whether it has effect on low temperature auto-ignition and oxidation of DME. Moreover, in the atmosphere, under the scenarios of low NOx, the H-shift provides an alternate route for DME oxidation without the involvement of NO/NO_2, also representing an autoxidation and self-cleaning of ethers. This process is also enhanced by $\dot{O}H$ recycling in the ethers oxidation.

4. Conclusions

Here we carried out a theoretical investigation of $CH_3O\dot{C}H_2 + O_2$ reactions, covering the full range of temperature and pressure found across both atmospheric and combustion. Geometries, frequencies, internal rotation models, single point energies and zero-point corrected energies were computed to construct the potential energy surface of $CH_3O\dot{C}H_2 + O_2$ system. Pressure-dependent rate coefficients have been computed for the reaction of $CH_3O\dot{C}H_2 + O_2$ PES using the RRKM/ME method with microcanonical variational transition state theory, and conventional transition state theory together with an Eckart tunneling correction is used to calculate high-pressure limit rate coefficients.

The $CH_3OCH_2O\dot{O}$ formation is absolute dominant channel for the reaction of $CH_3O\dot{C}H_2 + O_2$ at pressure above 1 atm, while the temperature has a controlling influence on the branching ratio of products at lower pressures ($\leq$ 1 atm). The rate coefficient of isomerization (from $CH_3OCH_2O\dot{O}$ to $\dot{C}H_2OCH_2O_2H$) at 1 atm is ~ 99 % of the HPL, however, the rate coefficient deviates more significantly from the HPL as the temperature increase, especially at lower pressures ($\leq$ 1 atm).

The formed $\dot{C}H_2OCH_2O_2H$ presents many possible decomposition pathways, the dominant and widely recognized channel is the channel generating $2CH_2O + \dot{O}H$. Two possible decomposition pathways of $\dot{C}H_2OCH_2O_2H$ to $2CH_2O + \dot{O}H$ are identified, first a scission of O—O bond or the C—O bond of $\dot{C}H_2O$—CH_2O_2H breaking first to eventually form two formaldehyde molecules and one hydroxyl radical. The former is more favourable since lone pair-lone pair repulsion between these two oxygen weakens the O—O bond relative the C—O bond, resulting in a lower barrier.

Another possible reaction channel of $\dot{C}H_2OCH_2O_2H$ assumed by Suzaki et al.[89], namely though reaction sequence $\dot{C}H_2OCH_2O_2H \rightarrow HOCH_2OCH_2\dot{O} \rightarrow H\dot{C}O + CH_2O + H_2O$, are found in the present calculation. However, this three-product channel ($CH_3O\dot{C}H_2 + O_2 = H\dot{C}O + CH_2O + H_2O$) do not appear to be as favourable.

The present calculation (only the entrance channel of the first O_2 addition mechanism in DME low-temperature chemistry) used directly in previously constructed reaction mechanisms were not necessarily lead to better agreement with experimental measurements (especially in the NTC region). Instead, incorporating the kinetics of all key reaction channels of $CH_3O\dot{C}H_2 + O_2$ reaction surface into previously constructed reaction mechanisms yields predictions that are in reasonable agreement with experimental measurements. It is because the kinetics parameters of $CH_3O\dot{C}H_2 + O_2$ system in previously constructed DME models are in a situation of compensation error. If only the kinetics of a single reaction channel is improved, it would inevitably lead to the amplification of errors in the kinetic parameters of other associated reaction, which would further affect the model performance.

Again, it's not the authors' intention to judge the quality of a model's description of detailed chemistry, and it is out of the scope of the present paper to consolidate modeling efforts. However, the purpose of this study is to provide the theoretical kinetic parameters of $CH_3O\dot{C}H_2 + O_2$ reactions and to verify whether it has effect on low temperature auto-ignition and oxidation of DME.

Associated Content

Supporting Information. The supporting information for this article is available free of charge on the WWW under https://doi.org/10.1002/cjoc.2023xxxxx.

Declaration of competing interest

The authors declare that they have no known competing financial interests or personal relationships that could have appeared to influence the work reported in this paper.

Acknowledgment

This work was supported by the Basic Science Center Program for Ordered Energy Conversion of the National Natural Science Foundation of China (Nos. 51888103), and the National Science and Technology Major Project (J2019-III-0004-0047 and 2021-JCJQ-ZD-062-12).

Supplementary materials

Supplementary material associated with this article can be found, in the online version, at doi:10.1016/j.combustflame.2024.113339.

References

[1] M. Ehn, J.A. Thornton, E. Kleist, M. Sipilae, H. Junninen, I. Pullinen, M. Springer, F. Rubach, R. Tillmann, B. Lee, A large source of low-volatility secondary organic aerosol, Nature 27 (506) (2014) 476–479.
[2] F. Paulot, J.D. Crounse, H.G. Kjaergaard, A. Kürten, J. Clair, J.H. Seinfeld, P. O. Wennberg, Unexpected epoxide formation in the gas-phase photooxidation of isoprene, Science 327 (5966) (2009) 730–733.
[3] M. Claeys, B. Graham, G. Vas, W. Wang, R. Vermeylen, V. Pashynska, J. Cafmeyer, P. Guyon, M.O. Andreae, P. Artaxo, Formation of secondary organic aerosols through photooxidation of isoprene, Science 303 (5661) (2004) 1173–1176.
[4] J. Tröstl, W.K. Chuang, H. Gordon, M. Heinritzi, C. Yan, U. Molteni, L. Ahlm, C. Frege, F. Bianchi, R. Wagner, M. Simon, K. Lehtipalo, The role of low-volatility organic compounds in initial particle growth in the atmosphere, Nature 533 (2016) 527–531.
[5] J.D. Crounse, L.B. Nielsen, S. Jørgensen, H.G. Kjaergaard, P.O. Wennberg, Autoxidation of organic compounds in the atmosphere, J. Phys. Chem. Lett 4 (20) (2013) 3513–3520.
[6] F. Bianchi, T. Kurtén, M. Riva, C. Mohr, M.P. Rissanen, P. Roldin, T. Berndt, J. D. Crounse, P.O. Wennberg, T.F. Mentel, J. Wildt, H. Junninen, T. Jokinen, M. Kulmala, D.R. Worsnop, J.A. Thornton, N. Donahue, H.G. Kjaergaard, M. Ehn, Highly oxygenated organic molecules (HOM) from gas-phase autoxidation involving peroxy radicals: a key contributor to atmospheric aerosol, Chem. Rev. 119 (6) (2019) 3472–3509.
[7] J. Zádor, C.A. Taatjes, R.X. Fernandes, Kinetics of elementary reactions in low-temperature autoignition chemistry, Prog. Energy Combust. Sci. 37 (4) (2011) 371–421.
[8] J.J. Orlando, G.S. Tyndall, Laboratory studies of organic peroxy radical chemistry: an overview with emphasis on recent issues of atmospheric significance, Chem. Soc. Rev. 41 (19) (2012) 6294–6317.
[9] M.J. Goldman, W.H. Green, J.H. Kroll, Chemistry of simple organic peroxy radicals under atmospheric through combustion conditions: role of temperature, pressure, and NOx level, J. Phys. Chem. A 125 (48) (2021) 10303–10314.
[10] K.H. Møller, T. Berndt, H.G. Kjaergaard, Atmospheric autoxidation of amines, Environ. Sci. Technol. 54 (18) (2020) 11087–11099.
[11] N. Hyttinen, H.C. Knap, M.P. Rissanen, S. Jørgensen, H.G. Kjaergaard, T. Kurtén, Unimolecular HO_2 loss from peroxy radicals formed in autoxidation is unlikely under atmospheric conditions, J. Phys. Chem. A 120 (20) (2016) 3588–3595.
[12] J.D. Crounse, F. Paulot, H.G. Kjaergaard, P.O. Wennberg, Peroxy radical isomerization in the oxidation of isoprene, Phys. Chem. Chem. Phys. 13 (30) (2011) 13607–13613.
[13] P.A. Glaude, N. Marinov, Y. Koshiishi, N. Matsunaga, M. Hori, Kinetic modeling of the mutual oxidation of NO and larger alkanes at low temperature, Energy Fuel 19 (5) (2005) 1839–1849.
[14] T.A. Semelsberger, R.L. Borup, H.L. Greene, Dimethyl ether (DME) as an alternative fuel, J. Power Sources 156 (2) (2006) 497–511.
[15] M.E Jenkin, G.D. Hayman, Photochemical ozone creation potentials for oxygenated volatile organic compounds: sensitivity to variations in kinetic and mechanistic parameters, Atmos. Environ 33 (8) (1999) 1275–1293.
[16] Sainan Wang, L. Wang, The atmospheric oxidation of dimethyl, diethyl, and diisopropyl ethers. The role of the intramolecular hydrogen shift in peroxy radicals, Phys. Chem. Chem. Phys. 18 (11) (2016) 7707–7714.
[17] J. Sehested, K. Sehested, J. Platz, H. Egsgaard, O.J. Nielsen, Oxidation of dimethyl ether: absolute rate constants for the self reaction of CH_3OCH_2 radicals, the reaction of CH_3OCH_2 radicals with O_2, and the thermal decomposition of CH_3OCH_2 radicals, Int. J. Chem. Kinet. 29 (8) (1997) 627–636.
[18] J. Sehested, T. Møgelberg, T.J. Wallington, E.W. Kaiser, F.M. Company, M. Drop, P. O. Box, Dimethyl ether oxidation: kinetics and mechanism of the $CH_3OCH_2 + O_2$ reaction at 296 K and 0.38–940 torr total pressure, J. Aerosol. Sci. 28 (6) (1996) 1104–1105.
[19] M.M. Maricq, J.J. Szente, J.D. Hybl, Kinetic studies of the oxidation of dimethyl ether and Its chain reaction with Cl_2, J. Phys. Chem. A 101 (28) (1997) 5155–5167.
[20] K. Suzaki, K. Tsuchiya, M. Koshi, A. Tezaki, Analysis of HO_2 and OH formation mechanisms using FM and UV spectroscopy in dimethyl ether oxidation, J. Phys. Chem. A 111 (19) (2007) 3776–3788.
[21] K. Hoyermann, F. Nacke, Elementary reactions of the methoxymethyl radical in the gas phase: CH_3OCH_3+F, CH_2OCH_3+CH_2OCH_3, CH_2OCH_3+O_2 and CH_2OCH_3+O, Symp. (International) Combust. 26 (1) (1996) 505–512.
[22] A.J. Eskola, S.A. Carr, R.J. Shannon, B. Wang, M.A. Blitz, M.J. Pilling, P. W. Seakins, S.H. Robertson, Analysis of the kinetics and yields of OH radical production from the $CH_3OCH_2 + O_2$ reaction in the temperature range 195–650 K: an experimental and computational study, J. Phys. Chem. A 118 (34) (2014) 6773–6788.
[23] C.M. Rosado-Reyes, J.S. Francisco, J.J. Szente, M. Matti Maricq, L.F. Østergaard, Dimethyl ether oxidation at elevated temperatures (295–600 K), J. Phys. Chem. A 109 (48) (2005) 10940–10953.
[24] A. Masaki, S. Tsunashima, N. Washida, Rate constants for reactions of substituted methyl radicals (CH_2OCH_3, CH_2NH_2, CH_2I, and CH_2CN) with O_2, J. Phys. Chem. 99 (35) (1995) 13126–13131.
[25] P.J. Stephens, F.J. Devlin, C.F. Chabalowski, M.J. Frisch, Ab initio calculation of vibrational absorption and circular dichroism spectra using density functional force fields, J. Phys. Chem. 98 (45) (1994) 11623–11627.
[26] A.D. McLean, G.S. Chandler, Contracted Gaussian basis sets for molecular calculations. I. Second row atoms, Z=11–18, J. Chem. Phys. 72 (10) (1980) 5639–5648, https://doi.org/10.1063/1.438980.
[27] R. Krishnan, J.S. Binkley, R. Seeger, J.A. Pople, Self-consistent molecular orbital methods. XX. A basis set for correlated wave functions, J. Chem. Phys. 72 (1) (1980) 650–654, https://doi.org/10.1063/1.438955.
[28] Y. Zhao, D.G. Truhlar, Density functionals with broad applicability in chemistry, Acc. Chem. Res. 41 (2) (2008) 157–167.
[29] T. Yanai, D.P. Tew, N.C. Handy, A new hybrid exchange-correlation functional using the coulomb-attenuating method (CAM-B3LYP), Chem. Phys. Lett. 393 (1–3) (2004) 51–57.
[30] L.F. Holroyd, T.V. Mourik, Insufficient description of dispersion in B3LYP and large basis set superposition errors in MP2 calculations can hide peptide conformers, Chem. Phys. Lett. 442 (1–3) (2007) 42–46.
[31] A.L. Garden, F. Paulot, J.D. Crounse, I.J. Maxwell-Carmeron, P.O. Wennberg, H. G. Kjaergaard, Calculation of conformationally weighted dipole moments useful in ion–molecule collision rate estimates, Chem. Phys. Lett. 474 (1–3) (2009) 45–50.
[32] N. Hyttinen, O. Kupiainen-Määttä, M.P. Rissanen, M. Muuronen, T. Kurtén, Modeling the charging of highly oxidized cyclohexene ozonolysis products using nitrate-based chemical ionization, J. Phys. Chem. A 119 (24) (2015) 6339–6345.
[33] M.P. Rissanen, T. Kurtén, M. Sipilä, J.A. Thornton, J. Kangasluoma, N. Sarnela, H. Junninen, S. Jørgensen, S. Schallhart, M.K. Kajos, R. Taipale, M. Springer, T. F. Mentel, T. Ruuskanen, T. Petäjä, D.R. Worsnop, H.G. Kjaergaard, M. Ehn, The formation of highly oxidized multifunctional products in the ozonolysis of cyclohexene, J. Am. Chem. Soc. 136 (44) (2014) 15596–15606.
[34] K.H. Møller, R.V. Otkjær, N. Hyttinen, T. Kurten, H.G. Kjaergaard, Cost-effective implementation of multiconformer transition state theory for peroxy radical hydrogen shift reactions, J. Phys. Chem. A 120 (2016) 10072–10087.
[35] E. Hansen, A.R. Rosales, B. Tutkowski, P.-O. Norrby, O. Wiest, Prediction of stereochemistry using Q2MM, Am. Chem. Soc. 49 (5) (2016) 996–1005.
[36] J.E. Eksterowicz, K.N. Houk, Transition-state modeling with empirical force fields, Chem. Rev. 93 (7) (1993) 2439–2461.
[37] Y. Zhao, D.G. Truhlar, The M06 suite of density functionals for main group thermochemistry, thermochemical kinetics, noncovalent interactions, excited states, and transition elements: two new functionals and systematic testing of four M06-class functionals and 12 other functionals, Theor. Chem. Acc. 120 1–3 (2008) 215–241.
[38] F. Weigend, R. Ahlrichs, Balanced basis sets of split valence, triple zeta valence and quadruple zeta valence quality for H to Rn: design and assessment of accuracy, Phys. Chem. Chem. Phys. 7 (18) (2005) 3297–3305.
[39] P. Deng, L. Wang, L. Wang, Mechanism of gas-phase ozonolysis of β-myrcene in the atmosphere, J. Phys. Chem. A 122 (2018) 3013–3020.
[40] S.-S PAN, L.-M. WANG, The atmospheric oxidation mechanism of o-Xylene initiated by hydroxyl radicals, Acta Phys.-Chim. Sin. 118 (45) (2015) 10778–10787.
[41] M.R. Dash, B. Rajakumar, Theoretical investigations of the gas phase reaction of limonene with OH radical, Mol. Phys. 113 (21) (2015) 1–14.
[42] R. Wu, S. Pan, Y. Li, L. Wang, Atmospheric oxidation Mechanism of toluene, J. Phys. Chem. A 118 (25) (2004) 4533–4547.
[43] P. Shanshan, W. Liming, Atmospheric oxidation mechanism of m-Xylene initiated by OH radical, J. Phys. Chem. A 118 (45) (2014) 10778–10787.
[44] G.D. Purvis, R.J. Bartlett, A full coupled-cluster singles and doubles model: the inclusion of disconnected triples, J. Chem. Phys. 76 (4) (1982) 1910–1918.
[45] T.H. Dunning, Gaussian basis sets for use in correlated molecular calculations. I. The atoms boron through neon and hydrogen, J. Chem. Phys. 90 (2) (1989) 1007–1023.
[46] D.G. Truhlar, Basis-set extrapolation, Chem. Phys. Lett. 294 (1–3) (1998) 45–48.
[47] J.M.L. Martin, Ab initio total atomization energies of small molecules — Towards the basis set limit, Chem. Phys. Lett. 259 (5–6) (1996) 669–678.
[48] D. Feller, D.A. Dixon, Extended benchmark studies of coupled cluster theory through triple excitations, J. Chem. Phys. 115 (8) (2001) 3484–3496.
[49] P.R. Taylor, T.J. Lee, A.P. Rendell, Comparison of the quadratic configuration interaction and coupled cluster approaches to electron correlation including the effect of triple excitations, J. Phys. Chem. 94 (14) (1990) 5463–5468.
[50] S.J. Klippenstein, L.B. Harding, Kinetics of the H+NCO reaction, Proc. Combust. Inst. 32 (1) (2009) 149–155.

[51] W. Győrffy, T. Shiozaki, G. Knizia, H.J. Werner, Analytical energy gradients for second-order multireference perturbation theory using density fitting, J. Chem. Phys. 138 (2013) 104104.
[52] T. Shiozaki, W. Gyorffy, P. Celani, H.J. Werner, Communication: extended multi-state complete active space second-order perturbation theory: energy and nuclear gradients, J. Chem. Phys. 135 (2011) 081106.
[53] P. Celani, H.J. Werner, Multireference perturbation theory for large restricted and selected active space reference wave functions, J. Chem. Phys. 112 (13) (2000) 5546–5557.
[54] E. Papajak, J. Zheng, X. Xu, H.R. Leverentz, D.G. Truhlar, Perspectives on basis sets beautiful: seasonal plantings of diffuse basis functions, J. Chem. Theory Comput. 7 (10) (2011) 3027–3034.
[55] J. Duan, J. Ji, L. Ye, Q. Meng, Y. Zhai, L. Zhang, Theoretical calculation of low-temperature oxidation of heptyl radicals and O_2, Combust. Flame 217 (2020) 274–284.
[56] C. Franklin Goldsmith, W.H. Green, S.J. Klippenstein, Role of O_2 + QOOH in low-temperature ignition of propane. 1. Temperature and pressure dependent rate coefficients, J. Phys. Chem. A 116 (13) (2012) 3323–3346.
[57] Y. Lili, Z. Lidong, Q. Fei, Ab initio kinetics on low temperature oxidation of iso-pentane: the first oxygen addition, Combust. Flame 190 (2018) 119–132.
[58] J. Foresman, J. Ortiz, J. Cioslowski, D. Fox, Gaussian 09, Revision D. 01, Gaussian, Inc., Wallingford, CT, 2009.
[59] H.J. Werner, P.J. Knowles, G. Knizia, F.R. Manby, M. Schütz, Molpro: a general-purpose quantum chemistry program package, Wires. Comput. Mol. Sci. 2 (2) (2012) 242–253.
[60] H.J. Werner; P.J. Knowles; G. Knizia; F.R. Manby; M. Schütz; and others, MOLPRO, Version 2019 .2, A Package of Ab Initio Programs, 2019.
[61] H.-J. Werner, P.J. Knowles, F.R. Manby, J.A. Black, K. Doll, A. Heßelmann, D. Kats, A. Köhn, T. Korona, D.A. Kreplin, Q. Ma, T.F. Miller; III, A. Mitrushchenkov, K. A. Peterson, I. Polyak, G. Rauhut, M. Sibaev, The molpro quantum chemistry package, J. Chem. Phys. 152 (14) (2020) 1441071–14410724.
[62] J.A. Miller, S.J. Klippenstein, Master equation methods in gas phase chemical kinetics, J. Phys. Chem. A 110 (36) (2006) 10528–10544.
[63] S.J. Klippenstein, J.A. Miller, From the time-dependent, multiple-well master equation to phenomenological rate coefficients, J. Phys. Chem. A 106 (40) (2002) 9267–9277.
[64] J.A. Miller, S.J. Klippenstein, Master equation methods in gas phase chemical kinetics, J. Phys. Chem. A 110 (36) (2006) 10528–10544.
[65] A. Fernandez-Ramos, J.A. Miller, S.J.K Lippenstein, D.G. Truhlar, Modeling the kinetics of bimolecular reactions, Chem. Rev. 106 (11) (2006) 4518–4584.
[66] C.F. Goldsmith, W.H. Green, S.J. Klippenstein, Role of O_2 + QOOH in low-temperature ignition of propane. 1. Temperature and pressure dependent rate coefficients, J. Phys. Chem. A 116 (13) (2012) 3325–3346.
[67] D.G. Truhlar Variational transition state theory: progress report, July 1, 1979-June 30.
[68] D.C. Clary, The theory of chemical reaction dynamics, 1986, p.ˆpp.
[69] I.M. Alecu, J. Zheng, Y. Zhao, D.G. Truhlar, Computational thermochemistry: scale factor databases and scale factors for vibrational frequencies obtained from electronic model chemistries, J. Chem. Theory Comput 6 (9) (2010) 2872–2887.
[70] E. Carl, The penetration of a potential barrier by electrons, Phys. Rev. 35 (11) (1930) 1303–1309.
[71] Y. Georgievskii, J.A. Miller, M.P. Burke, S.J. Klippenstein, Reformulation and solution of the master equation for multiple-well chemical reactions, J. Phys. Chem. A 117 (46) (2013) 12146–12154, https://doi.org/10.1021/jp4060704.
[72] L. Tian, C. Feiwu, Multiwfn: a multifunctional wavefunction analyzer, J. Comput. Chem. 33 (2012) 580–592.
[73] T. Lu, F. Chen, Calculation of molecular orbital composition, Acta Phys-Chim. Sin. 69 (2011) 2393–2406.
[74] W. Humphrey, A. Dalke, K. Schulten, VMD: visual molecular dynamics, J. Mol. Graph. 14 (1996) 33–38.
[75] A. Andersen, E.A. Carter, A hybrid density functional theory study of the low-temperature dimethyl ether combustion pathways. I: chain-propagation, Israel J. Chem. 42 (2–3) (2003) 245–260.
[76] T. Yamada, J.W. Bozzelli, T.H. Lay, Comparisons of CBS-q and G2 calculations on thermodynamic properties, transition states, and kinetics of dimethyl-ether + O2 reaction system, Int. J. Chem. Kinet. 32 (7) (2000) 435–452.
[77] A. Rodriguez, O. Frottier, O. Herbinet, R. Fournet, R. Bounaceur, C. Fittschen, F. Battin-Leclerc, Experimental and modeling investigation of the low-temperature oxidation of dimethyl ether, J. Phys. Chem. A 119 (28) (2015) 7905–7923.
[78] Y. Li, C.W. Zhou, K.P. Somers, K. Zhang, H.J. Curran, The oxidation of 2-butene: a high pressure ignition delay, kinetic modeling study and reactivity comparison with isobutene and 1-butene, Proc. Combust. Inst. (2016) S1540748916300529.
[79] A.J. Eskola, S.A. Carr, M.A. Blitz, M.J. Pilling, P.W. Seakins, Kinetics and yields of OH radical from the CH_3OCH_2+O_2 reaction using a new photolytic source, Chem. Phys. Lett. 487 (1–3) (2010) 45–50.
[80] H.J. Curran, W.J. Pitz, C.K. Westbrook, P. Dagaut, J.-C. Boettner, M. Cathonnet, A wide range modeling study of dimethyl ether oxidation, Int. J. Chem. Kinet. 30 (3) (1998) 229–241.
[81] Z. Zhao, M. Chaos, A. Kazakov, F.L. Dryer, Thermal decomposition reaction and a comprehensive kinetic model of dimethyl ether, Int. J. Chem. Kinet. 40 (1) (2008) 1–18.
[82] U. Burke, K. P.Somers, P.O. Toole, C.M. Zinner, N. Marquet, G. Bourque, E. L. Petersen, W.K. Metcalfe, Z. Serinyel, H.J. Curran, An ignition delay and kinetic modeling study of methane, dimethyl ether, and their mixtures at high pressures, Combust. Flame 162 (2) (2015) 315–330.
[83] Z. Wang, X. Zhang, L. Xing, L. Zhang, F. Herrmann, K. Moshammer, F. Qi, K. Kohse-Hoeinghaus, Experimental and kinetic modeling study of the low- and intermediate-temperature oxidation of dimethyl ether, Combust. Flame 162 (4) (2015) 1113–1125.
[84] E.E. Dames, A.S. Rosen, B.W. Weber, C.W. Gao, C.-J. Sung, W.H. Green, A detailed combined experimental and theoretical study on dimethyl ether/propane blended oxidation, Combust. Flame 168 (2016) 310–330.
[85] C.B. Reuter, R. Zhang, O.R. Yehia, Y. Rezgui, Y. Ju, Counterflow flame experiments and chemical kinetic modeling of dimethyl ether/methane mixtures, Combust. Flame 196 (2018) 1–10.
[86] H. Hashemi, J.M. Christensen, P. Glarborg, High-pressure pyrolysis and oxidation of DME and DME/CH_4, Combust. Flame 205 (2019) 80–92.
[87] A. Andersen, E.A. Carter, First-principles-derived kinetics of the reactions involved in low-temperature dimethyl ether oxidation, Mol. Phys. 106 (2–4) (2008) 367–396.
[88] R. Chemkin-Pro, 15112, Reaction Design, Reaction Design, in: R. CHEMKIN-PRO (Ed.) Inc., San Diego, CA, 2011.
[89] K. Suzaki, K. Tsuchiya, M. Koshi, A. Tezaki, Analysis of HO_2 and OH formation mechanisms using FM and UV spectroscopy in dimethyl ether oxidation, J. Phys. Chem. A 111 (19) (2007) 3776–3788.